

Joule-Thomson effect and Efficiency of deformed AdS-Schwarzschild black hole in presence of quintessence

Dhruba Jyoti Gogoi^{1,2,*}, Ronit Karmakar^{3,†}, Jyatsnasree Bora^{1,4,‡}, Pohar Buragohain^{3,§} and Chandika Gogoi^{3,¶}

¹*Department of Physics, Madhabdev University, Narayanpur, Lakhimpur 784164, Assam, India*

²*Research Center of Astrophysics and Cosmology, Khazar University, Baku, AZ1096, 41 Mehseti Street, Azerbaijan*

³*Department of Physics, Moran College, Moranhat, Charaideo 785670, Assam, India*

⁴*Pacif Institute of Cosmology and Selfology (PICS) Sagara, Sambalpur 768224, Odisha, India*

We study the Joule–Thomson expansion and extended thermodynamics of a modified black hole characterised by the parameters α , β , and σ . Analysis of the Hawking temperature, Joule–Thomson coefficient, inversion curves, and isenthalpic trajectories shows that these parameters significantly modify the heating–cooling behaviour and thermal stability of the system. The deformation parameter α and control parameter β shift the temperature minimum, enlarge the cooling region, and raise the inversion temperature, while σ produces a weaker but consistent influence. The heat-engine analysis reveals that α enhances efficiency, whereas higher β and σ reduce it. Overall, the results demonstrate that geometric deformation and quintessence jointly govern the unified thermodynamic structure of the black hole.

Keywords: Deformed black hole; Black hole thermodynamics; Joule Thomson Cooling; Quintessence

I. INTRODUCTION

Black holes constitute regions of spacetime where gravitational attraction is sufficiently intense to prevent the escape of particles and electromagnetic radiation. At their centre, both density and curvature diverge, giving rise to a singularity. The process of crossing the event horizon is therefore irreversible [1]. More than a century ago, in 1915, Einstein formulated General Relativity (GR) [2]. Although extraordinarily successful, GR exhibits well-known limitations: it predicts physical singularities such as those at the centres of black holes where the theory ceases to remain valid, it fails to reconcile with quantum mechanics, and it relies on unobserved components like Dark Matter (DM) and Dark Energy (DE) [3]. Consequently, despite its remarkable empirical successes, GR is not regarded as the ultimate or complete description of gravitation [3].

A transformative development in gravitational physics is the realisation that black holes behave as thermodynamic systems, fundamentally altering our understanding of GR and its interface with Quantum Field Theory (QFT) [4–10]. Classical black holes, characterised solely by mass, charge, and angular momentum, obey dynamical laws that closely mirror the four laws of thermodynamics. This correspondence gained physical significance when Bekenstein proposed that black holes possess entropy, motivated by the paradox that ordinary entropy appears to be lost when matter falls into a black hole [11]. To preserve the second law of thermodynamics, he introduced the notion that black hole entropy is proportional to the surface area of the event horizon [11]. This led to the formulation of the Generalised Second Law (GSL), which asserts that the sum of ordinary entropy and black hole entropy never decreases, thereby resolving the apparent entropy loss paradox. Black holes also exhibit negative specific heat, preventing them from attaining stable thermal equilibrium with an arbitrarily large heat bath and complicating attempts to employ standard statistical-mechanical ensembles in gravitational contexts [12]. Recently, the topology of black hole thermodynamics has also received some attention from researchers [10, 13–16].

The Joule–Thomson (J–T) expansion provides an important thermodynamic framework to investigate a thermal system as well as black hole systems in different modified theories of gravity. In this process, a gas initially at high pressure expands through a porous barrier into a region of lower pressure while maintaining constant enthalpy. For black holes, enthalpy corresponds to the mass [9, 17–19]. The J–T expansion allows one to examine heating–cooling behaviour and derive inversion temperatures. The temperature variation with respect to pressure at constant enthalpy is quantified by the J–T coefficient, $\mu = \left(\frac{\partial T}{\partial P}\right)_H$, whose sign determines whether the system heats or cools during expansion. Although pressure variation is always negative during expansion, the temperature variation may assume either sign depending on the characteristics of the system. A positive temperature change implies a negative J–T coefficient, indicating heating, whereas a negative temperature change associated with a positive J–T coefficient signals cooling. At the inversion temperature T_i , the coefficient μ vanishes. The corresponding pressure is the inversion pressure (P_i), and the point (T_i, P_i) marks the transition between heating and cooling regimes. Regions above the inversion curve correspond to cooling, whereas regions below correspond to heating [17].

* Email: moloydhruba@yahoo.in

† Email: ronit.karmakar622@gmail.com

‡ Email: jyatsnasree.borah@gmail.com

§ Email: buragohainpohar@gmail.com

¶ Email: gogoichandika63@gmail.com

Extensive studies have established that the temperature–pressure (T–P) diagram provides a robust diagnostic tool for distinguishing heating and cooling regions [20–32]. In a detailed treatment of J–T expansion for black holes in Einstein gravity was presented by Ökcü and Aydiner [17], who analysed the J–T effect for charged AdS black holes and identified both parallels and departures from Van der Waals fluids. Their subsequent work extended the analysis to Kerr–AdS black holes within the extended phase space [33], effectively characterising cooling and heating regions from the T–P diagram. Later studies generalised these ideas to quintessence holographic superfluids of Reissner–Nordström black holes in $f(R)$ gravity [34, 35]. The influence of spacetime dimensionality on J–T expansion was examined in Ref. [35]. Furthermore, the J–T expansion of charged accelerating AdS black holes in $f(R)$ gravity demonstrated that the inversion curve consistently corresponds to the lower branch, implying that the black hole remains in a cooling regime throughout expansion [36]. Quantum-corrected Schwarzschild–AdS black holes surrounded by quintessence have also been analysed to explore their thermodynamic and shadow properties [37].

Recent investigations of black holes in metric-affine gravity reveal that inversion temperature and pressure increase with the strength of metric-affine corrections, while they decrease with the charge (q_e) [38]. Higher-dimensional charged dilatonic black holes with potential $V(\phi)$ have similarly been studied, highlighting the influence of dimensionality and dilaton parameters on J–T behaviour [39]. Studies of charged AdS black holes surrounded by modified Chaplygin gas show that the divergence point and zero point of the J–T coefficient shift rightward as charge increases [40]. Another work [41] discusses the Joule-Thomson expansion and thermodynamics of a non-linear charged AdS black hole solution, and analyses the effect of model parameters on the inversion curves. Ref. [42] uses a simplified framework for thermodynamic geometry of AdS black holes in Einstein Maxwell scalar theory, constructing consistent geometric descriptions across phase spaces and examining stability under thermal fluctuations, extending the analysis to regularized Lovelock theory. These works collectively inspired a substantial body of literature on J–T expansion across diverse black hole geometries [20–32, 36, 39, 43–79].

Parallel to these developments, black holes have also been conceptualised as working substances in thermodynamic heat engines. Holographic black hole heat engines, capable of performing mechanical work, have been analysed extensively in [80]. Rotating black hole heat engines extract mechanical work from the rotational energy stored in the ergosphere [81]. Additional analyses of efficiency and work extraction for a variety of black hole heat engine models appear in [75, 82–89]. Of particular note, Ref. [90] examined the efficiency and Carnot efficiency of Bardeen–AdS black hole heat engines and demonstrated that quintessence fields enhance thermodynamic efficiency.

With this brief review of the relevant literature, the present study investigates the thermodynamic properties, J–T expansion, and heat engine efficiency of deformed AdS-Schwarzschild black holes in a quintessence background. As mentioned earlier, constructing regular, non-singular black hole models is a critical step toward a complete gravitational theory. In this context, the deformed black hole geometry investigated in this work is not proposed as the final, fundamental theory of quantum gravity, but rather as a highly effective and necessary phenomenological testbed. By introducing a deformation parameter α to ensure the rapid asymptotic decay of the central energy density, and a control parameter β to encode nonlinear regularization effects, this model captures the essential, non-singular features expected from quantum-corrected gravity. Furthermore, by embedding this regularized core within a quintessence field σ , a physically realistic macroscopic environment compatible with a dark-energy-dominated universe has been constructed. Investigating the extended thermodynamics and Joule-Thomson expansion of this configuration allows us to identify how microscopic regularisations manifest as macroscopic thermodynamic signatures. Ultimately, this approach provides crucial theoretical clues, demonstrating how intrinsic geometric deformations and external exotic matter fields jointly reshape the thermal evolutionary tracks of black holes, offering concrete phase-space behaviours that cannot be obtained in standard GR.

After the introduction section, we have arranged the rest of the work in this manner: In Section II, we have discussed the black hole solution of the deformed AdS black hole in the presence of a quintessence field. In Section III, we examine the thermodynamic properties of the black hole and mainly the Joule-Thomson effect of the black hole. Next, the efficiency of the black hole is determined in Section IV. Section V presents our conclusions about our findings for black hole thermodynamics and its efficiency. Throughout this work, we use the natural unit system $G = c = \hbar = 1$ and the metric sign convention $(-, +, +, +)$.

II. DEFORMED ADS-SCHWARZSCHILD BLACK HOLE IN PRESENCE OF QUINTESSENCE

To obtain the deformed AdS-Schwarzschild black hole solution, we start with the four-dimensional action as [91]

$$A = \int d^4x \sqrt{-g} \left(\frac{R - 2\Lambda}{2\kappa} + \mathcal{L}_m + \mathcal{L}_X \right). \quad (1)$$

In this expression, the term g is the determinant of the metric, R is the Ricci scalar, and Λ represents the cosmological constant. Also $\kappa = 8\pi$. The Lagrangian density terms, \mathcal{L}_m and \mathcal{L}_X refer to the matter Lagrangian and Lagrangian for theories other than General Relativity (GR) or extra fields like tensor, scalar, or vector fields, respectively.

Varying this action (1) with respect to the metric, one can obtain the field equation as

$$G_{\mu\nu} + \Lambda g_{\mu\nu} = \kappa T_{\mu\nu}^{(\text{tot})}, \quad (2)$$

here $G_{\mu\nu}$ is representing the Einstein tensor; $T_{\mu\nu}^{(\text{tot})}$ stands for the total energy-momentum tensor:

$$T_{\mu\nu}^{(\text{tot})} = T_{\mu\nu}^{(\text{m})} + T_{\mu\nu}^{(\text{X})}. \quad (3)$$

$T_{\mu\nu}^{(\text{tot})}$ is the sum of matter and additional fields' energy-momentum tensor, which has the functional forms respectively

$$T_{\mu\nu}^{(\text{m})} = -\frac{2}{\sqrt{-g}} \frac{\delta(\sqrt{-g}L_m)}{\delta g^{\mu\nu}}, \quad (4)$$

and

$$T_{\mu\nu}^{(\text{x})} = -\frac{2}{\sqrt{-g}} \frac{\delta(\sqrt{-g}L_x)}{\delta g^{\mu\nu}}. \quad (5)$$

For a static and spherically symmetric spacetime, we use the metric function as

$$ds^2 = -e^{\nu(r)} dt^2 + e^{\mu(r)} dr^2 + r^2(d\theta^2 + \sin^2\theta d\phi^2). \quad (6)$$

As usual, t and r stand for the time and space coordinates, respectively, and θ and ϕ are polar and azimuthal angles.

To obtain the required black hole solution, following the article [91], we shall implement the Kerr-Schild condition [92]:

$$e^{\mu(r)} = e^{-\nu(r)}. \quad (7)$$

Also, to assimilate the deformation condition, one can introduce an energy density function as [91]:

$$\mathcal{E}(r) = \frac{\alpha}{\kappa(\beta + r)^4}. \quad (8)$$

Here, the term β is a constant parameter which controls the behaviour of the energy density at $r = 0$, and α stands for the deformation parameter which is responsible for a rapid asymptotic decay, and it avoids a central singularity. The specific algebraic form of this energy density is strictly motivated by the fundamental physical requirement to resolve the central curvature singularity inherent in the standard GR framework. In this context, the control parameter β acts as a necessary short-distance regularisation scale. Conceptually analogous to a minimal length cutoff predicted by effective quantum gravity approaches, it ensures that as the radial coordinate approaches the centre ($r \rightarrow 0$), the energy density remains finite rather than diverging to infinity. Simultaneously, the deformation parameter α dictates the strength of this non-singular deviation and enforces a rapid asymptotic decay, ensuring the geometry recovers its standard behaviour at large distances. Consequently, these parameters are not merely arbitrary mathematical artefacts; rather, they serve as physically motivated, effective corrections that capture the macroscopic phenomenological behaviour expected from a regularised, quantum-corrected black hole interior.

Now using Eq. 8 in the field equation, the metric function $B(r)$ can be obtained as

$$B(r) = \frac{\frac{\alpha\beta^2}{3(\beta+r)^3} + \frac{\alpha}{\beta+r} - \frac{\alpha\beta}{(\beta+r)^2} + \frac{r^3+c_1}{l^2} + r}{r(1 - 2M/r + r^2/l^2)}, \quad (9)$$

In this expression, M represents the ADM mass, $l = \sqrt{3/|\Lambda|}$ is the AdS radius, and c_1 is an integration constant having the value $-2Ml^2$. From this equation we can have:

$$e^{\zeta(r)} B(r) = 1 - \frac{2M}{r} + \frac{r^2}{l^2} + \alpha \frac{\beta^2 + 3r^2 + 3\beta r}{3r(\beta + r)^3} \equiv F(r). \quad (10)$$

Thus, the final line element for the deformed AdS-Schwarzschild black hole reads:

$$ds^2 = -F(r)dt^2 + \frac{1}{F(r)}dr^2 + r^2(d\theta^2 + \sin^2\theta d\phi^2). \quad (11)$$

This metric characterises a black hole solution having a deformation parameter α that includes alterations consistent with additional gravitational fields while maintaining the asymptotic AdS behaviour. With this solution, we will now incorporate the deformed Schwarzschild black hole surrounded by a field of quintessence in the AdS background [93]. To do so, one can attach the term $(\frac{\sigma}{r^{3\omega_q+1}})$, where σ represents a normalization factor associated with the quintessence and ω_q is a state parameter that satisfies the constraint condition, $\omega_q \in (-1, -1/3)$.

Thus, the reformed metric function is:

$$F(r) = 1 - \frac{2M}{r} + \frac{r^2}{l^2} + \alpha \frac{\beta^2 + 3r^2 + 3\beta r}{3r(\beta + r)^3} + \frac{\sigma}{r^{3\omega_q + 1}}. \quad (12)$$

In our investigation, we shall use $\omega_q = -2/3$.

In a recent study, a deformed black hole surrounded by both quintessence and a global monopole has been investigated [94]. The above solution is a special case of this solution in the absence of a global monopole. In the following part of our investigation, we shall use this black hole spacetime to study the thermodynamic behaviour, including the Joule-Thomson effect and thermodynamic efficiency.

III. THERMODYNAMICS AND JOULE-THOMSON EFFECT

The Hawking temperature is a fundamental thermodynamic quantity associated with black hole radiation. It is given by [95],

$$T_H = \frac{\kappa}{2\pi}, \quad (13)$$

where κ is the surface gravity given by,

$$\kappa = -\frac{1}{2} \frac{\partial_r g_{tt}}{\sqrt{-g_{tt}g_{rr}}} \Big|_{r=r_h}. \quad (14)$$

Here g_{tt} is the temporal coefficient and g_{rr} is the spatial coefficient. The term r_h represents the event horizon of the black hole. This results in a finding that the assumption that a black hole is completely black is not true, but it emits thermal radiation, which is known as Hawking radiation.

For the black hole defined by the metric function (12), the Hawking temperature is calculated as,

$$T_H = \frac{1}{4} \left(8Pr_h + \frac{2\sigma - \frac{\alpha r_h}{(\beta + r_h)^4}}{\pi} + \frac{1}{\pi r_h} \right). \quad (15)$$

In the above expression, P is the pressure associated with the black hole spacetime given by,

$$P = -\frac{\Lambda}{8\pi}. \quad (16)$$

We can now use the expressions of Hawking temperature and pressure to obtain the J-T coefficient associated with the black hole spacetime. As mentioned earlier, the J-T expansion is a thermodynamic process which provides us insight into the temperature behaviour of a system undergoing adiabatic expansion. During the J-T expansion, the enthalpy, which is the mass of a black hole, M , is constant, making it an isenthalpic process. This allows us to study the temperature changes of the black hole system that result solely from the variations in pressure and volume. The Joule-Thomson coefficient is given by:

$$\mu = \left(\frac{\partial T}{\partial P} \right)_M = \frac{1}{C_p} \left[T \left(\frac{\partial V}{\partial T} \right)_P - V \right] = \frac{(\partial T / \partial r_h)_M}{(\partial P / \partial r_h)_M} \quad (17)$$

Here C_p represents the heat capacity at constant pressure of the black hole system. Expression of C_p is given by,

$$C_p = \frac{2\pi r_h \left(8Pr_h + \left(2\sigma - \frac{\alpha r_h}{(\beta + r_h)^4} + \frac{1}{r_h} \right) \pi^{-1} \right)}{\frac{\alpha(3r_h - \beta)}{\pi(\beta + r_h)^5} - \frac{1}{\pi r_h^2} + 8P}. \quad (18)$$

A positive J-T coefficient ($\mu > 0$) indicates cooling upon expansion, while a negative value ($\mu < 0$) corresponds to heating. The following equation shows the slope of the P-T graph for the AdS-deformed black hole surrounded by a quintessence field (with $\omega = -2/3$),

$$\mu = \frac{2\pi r_h^2 \left(8P - \left(\frac{\alpha}{(\beta + r_h)^4} - \frac{4\alpha r_h}{(\beta + r_h)^5} + \frac{1}{r_h^2} \right) \pi^{-1} \right) \left(\frac{3 \left(8Pr_h + \left(-\frac{\alpha r_h}{(\beta + r_h)^4} + \frac{1}{r_h} + 2\sigma \right) \pi^{-1} \right)}{8P - \left(\frac{\alpha}{(\beta + r_h)^4} - \frac{4\alpha r_h}{(\beta + r_h)^5} + \frac{1}{r_h^2} \right) \pi^{-1}} - r_h \right)}{3 \left(r_h \left(8\pi Pr_h - \frac{\alpha r_h}{(\beta + r_h)^4} + 2\sigma \right) + 1 \right)}. \quad (19)$$

The inversion temperature T_i is defined by the equation $\mu(T_i) = 0$. The inversion temperature separates cooling and heating processes. Using the definition of T_i and μ , we have,

$$T_i = V \left(\frac{\partial T}{\partial V} \right)_P = \frac{r_h}{3} \left(\frac{\partial T}{\partial r_h} \right)_P. \quad (20)$$

For the considered deformed AdS-Schwarzschild black hole in the presence of quintessence, the inversion temperature is calculated as,

$$T_i = - \frac{\beta^5 - 2r_h^3(\alpha - 5\beta^2(\beta\sigma + 1)) + \beta^4(\beta\sigma + 5)r_h + 5\beta^3(\beta\sigma + 2)r_h^2 + (5\beta\sigma + 1)r_h^5 + 5\beta(2\beta\sigma + 1)r_h^4 + \sigma r_h^6}{4\pi r_h(\beta + r_h)^5}. \quad (21)$$

At inversion pressure P_i , μ equals to zero and therefore P_i has the following form:

$$P_i = - \frac{2\beta^5 - \alpha\beta r_h^2 - 3\alpha r_h^3 + 10\beta^4 r_h + 20\beta^3 r_h^2 + 20\beta^2 r_h^3 + 3\sigma r_h(\beta + r_h)^5 + 10\beta r_h^4 + 2r_h^5}{8\pi r_h^2(\beta + r_h)^5}. \quad (22)$$

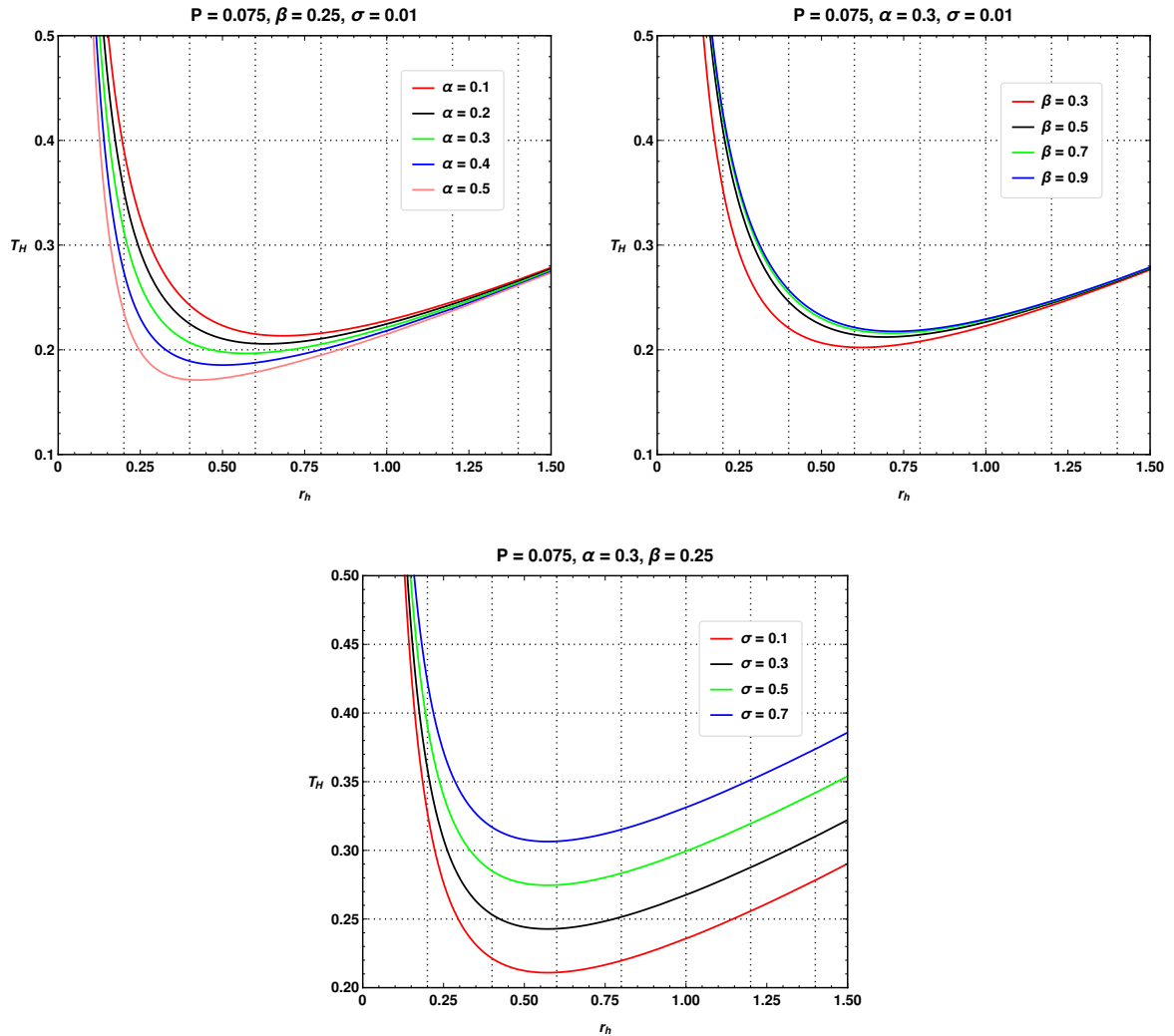


FIG. 1: Variation of Hawking temperature with horizon radius of the black hole.

Figure 1 illustrates the behaviour of the Hawking temperature T_H as a function of the horizon radius r_h for different values of the deformation parameter α , control parameter β , and the quintessence parameter σ . In all cases, the temperature exhibits a characteristic non-monotonic profile: it diverges in the limit of small horizon radius, decreases to a local minimum, and

subsequently grows for larger r_h . This generic structure indicates the presence of a thermodynamic transition between the small and large-horizon phases. The top-left panel displays the influence of α , showing that larger values of the deformation parameter lower the minimum temperature and shift its location toward smaller horizon radii. This behaviour reflects the contribution of α to the effective repulsive structure in the near-horizon geometry, thereby altering the stability properties of the black hole.

The influence of the control parameter β is shown in the top-right panel. As β increases, the temperature curves are slightly elevated, and the temperature minimum becomes shallower and occurs at marginally larger radii. This suggests that β , which typically encodes nonlinear or regularisation effects, moderates the drop in temperature in the intermediate region, effectively enhancing thermodynamic stability. The modification introduced by β becomes more pronounced in the small-radius regime, where nonlinear corrections are strongest, demonstrating its role in controlling the effective gravitational response of the system.

The bottom panel displays the effect of the quintessence parameter σ . Increasing σ results in a higher temperature in both the small and intermediate-radius regimes. The resulting upward shift in T_H underscores the thermodynamic sensitivity of the black hole to its external environment. Altogether, the three panels show that the parameters α , β , and σ significantly influence the thermal and stability characteristics of the black hole, especially in the region where geometric and matter-field corrections are non-negligible.

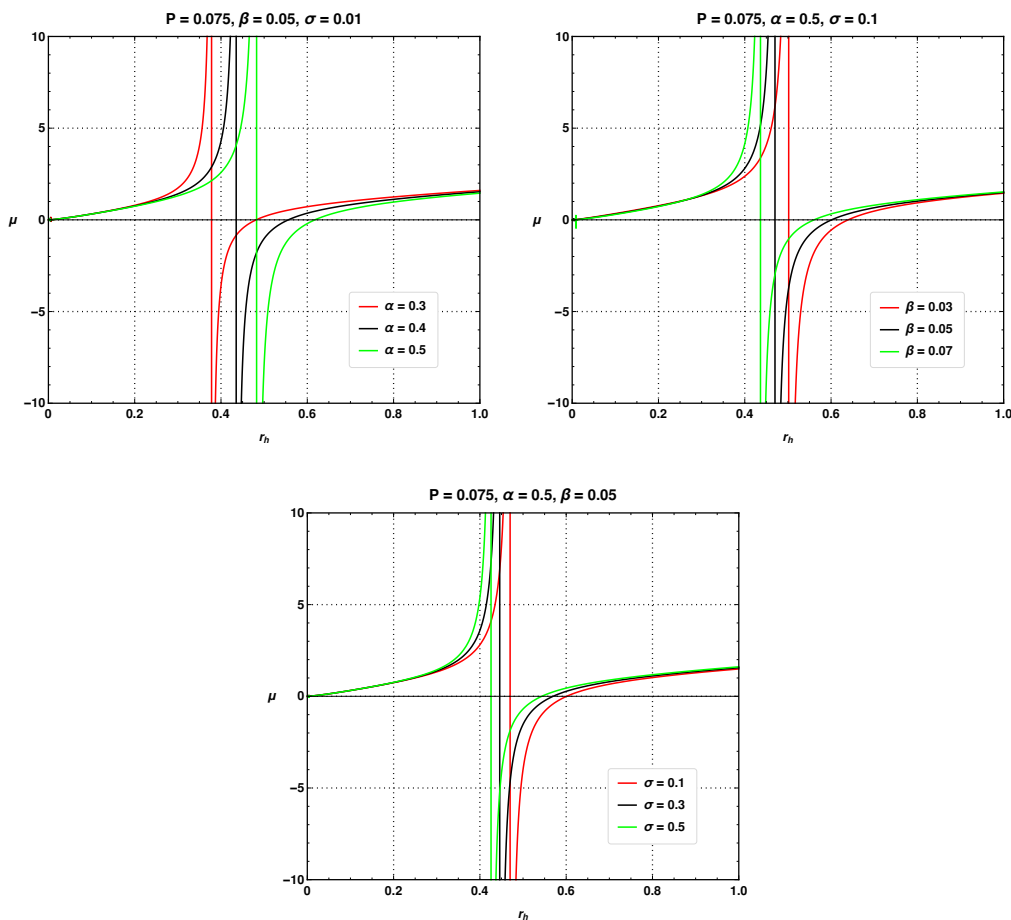


FIG. 2: JT coefficient vs event horizon radius of the black hole.

Figure 2 presents the behaviour of the Joule–Thomson coefficient μ as a function of the event horizon radius r_h for different combinations of the deformation parameter α , control parameter β , and quintessence parameter σ . In each panel, the Joule–Thomson coefficient exhibits a characteristic divergence at a critical radius, corresponding to the point where the slope of the Hawking temperature with respect to pressure changes its sign. The region where $\mu > 0$ indicates the cooling phase of the black hole during an isenthalpic expansion, whereas $\mu < 0$ corresponds to the heating phase. The presence of both positive and negative branches, therefore, marks the transition from heating to cooling, analogous to the van der Waals gas in ordinary thermodynamics. The sharpness and position of these divergences demonstrate that the black hole response to J-T expansion is highly sensitive to the underlying parameters of the theory.

The first two panels show the influence of α and β on $\mu(r_h)$. Increasing the deformation parameter α shifts the divergence point of μ toward larger radii and broadens the region over which μ remains positive, indicating that stronger deformation

enhances the cooling regime and delays the transition to heating. Similarly, an increase in β produces a comparable shift, though typically with a weaker effect. These trends are in clear agreement with the temperature profiles shown in Fig. 1, where larger values of α or β were found to displace the minimum of the temperature curve to larger horizon radii. Since the inversion point in the Joule–Thomson process coincides with the minimum of the temperature for isenthalpic trajectories, the parallel behaviour of $T_H(r_h)$ and $\mu(r_h)$ confirms the internal thermodynamic consistency of the model.

The bottom panel highlights the effect of the quintessence parameter σ . Increasing σ causes the divergence of μ to move to a larger horizon radius, while simultaneously enhancing the magnitude of both the heating and cooling branches. This behaviour directly reflects the upward shift in the Hawking temperature curves observed previously: larger σ increases the overall temperature of the black hole at small and intermediate radii, thereby modifying the location of the temperature minimum and the corresponding inversion radius. The consistent correlation between the temperature curves and the Joule–Thomson coefficient demonstrates that the parameters α , β , and σ collectively reshape the thermal landscape of the black hole. Together, the figures confirm that both the cooling–heating transition and the inversion mechanism are tightly governed by the same structural features of the black-hole geometry and its surrounding matter fields.

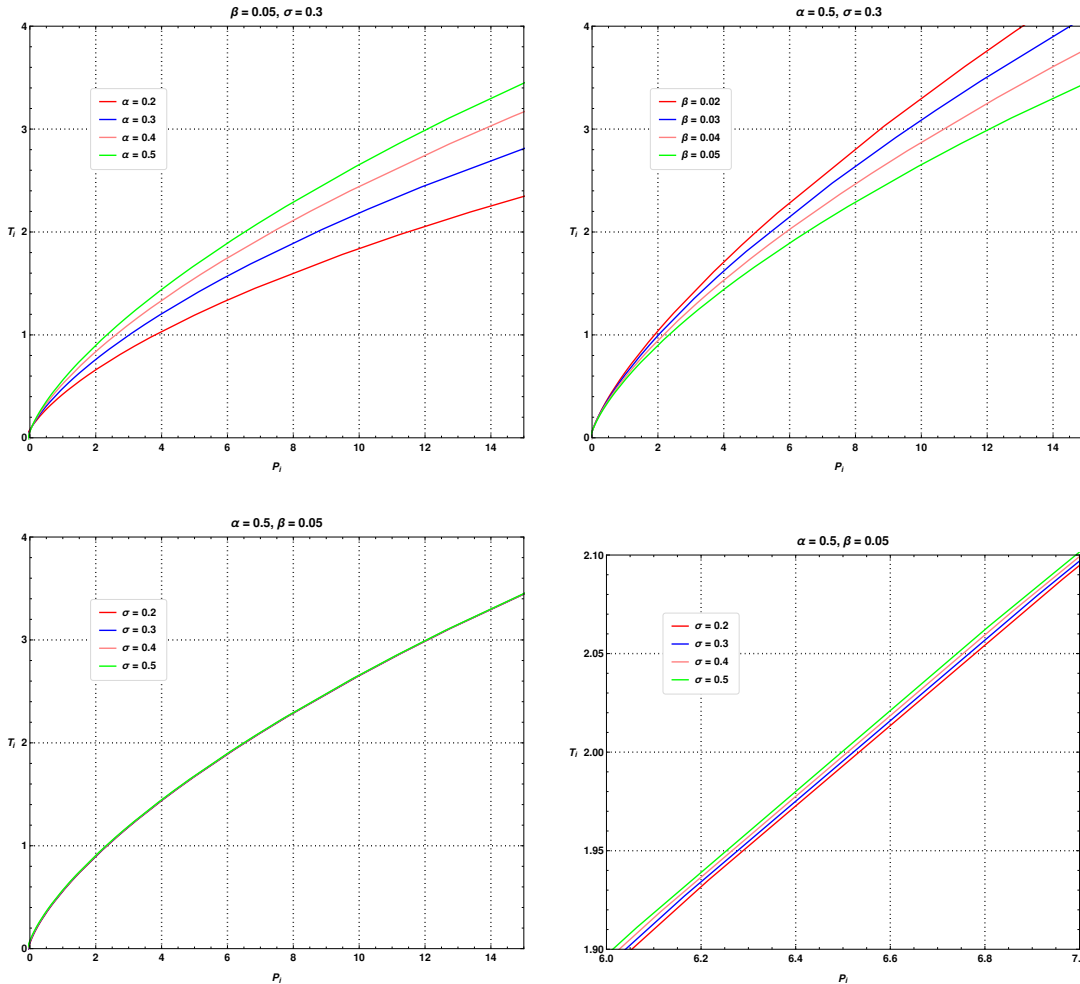


FIG. 3: Inversion curves of the black hole.

Figure 3 displays the inversion curves of the black hole for different values of the parameters α , β , and σ . The inversion temperature T_i marks the boundary between heating ($\mu < 0$) and cooling ($\mu > 0$) during the J-T expansion, and therefore encodes crucial information about the thermodynamic response of the system. In all panels, the inversion temperature increases monotonically with the inversion pressure P_i , reflecting the characteristic behaviour familiar from van der Waals fluids. The first figure demonstrates the influence of α , showing that larger values of the deformation parameter shift the inversion curve upward. This indicates that a stronger deformation increases the temperature at which the cooling–heating transition occurs. This trend is consistent with the behaviour observed in both the temperature and J-T coefficient plots: increasing α moves the temperature minimum to a larger radius and enhances the cooling region, thereby requiring a higher inversion temperature to trigger the transition.

The effect of the control parameter β is illustrated in the second panel. Similar to α , increasing β raises the inversion temperature across the full pressure range, although the shift is comparatively weaker. Since β typically controls the strength of nonlinear or regularisation effects in the underlying geometry, its influence on the inversion curve reflects modifications to the repulsive contributions in the thermodynamic equation of state. These results reinforce the trends previously observed in Fig. 1 and Fig. 2: larger β flattens the temperature profile, shifts the critical radius associated with the temperature minimum, and moderately alters the divergence structure of $\mu(r_h)$. The corresponding upward shift in T_i is therefore a natural thermodynamic consequence of the interplay between β and the near-horizon modifications introduced by the matter sector.

The final two panels show the effect of the quintessence parameter σ . The third figure reveals a slight increase in the inversion temperature as σ grows, while the fourth figure provides a zoomed-in view confirming that the influence of σ on the inversion curve is positive but extremely small. This behaviour is fully consistent with the earlier findings: in Fig. 1, increasing σ raised the Hawking temperature, particularly in the small- and intermediate-radius regions, while Fig. 2 demonstrated that σ shifts the divergence of the Joule–Thomson coefficient toward larger radii. Since the inversion temperature is determined by the condition $\mu = 0$, these changes naturally translate to a mild upward shift in T_i . However, the comparatively weaker dependence on σ indicates that the external quintessence-like field does not significantly modify the compressibility or microstructure of the black hole, leading to only minimal changes in its expansion-driven thermodynamic behaviour.

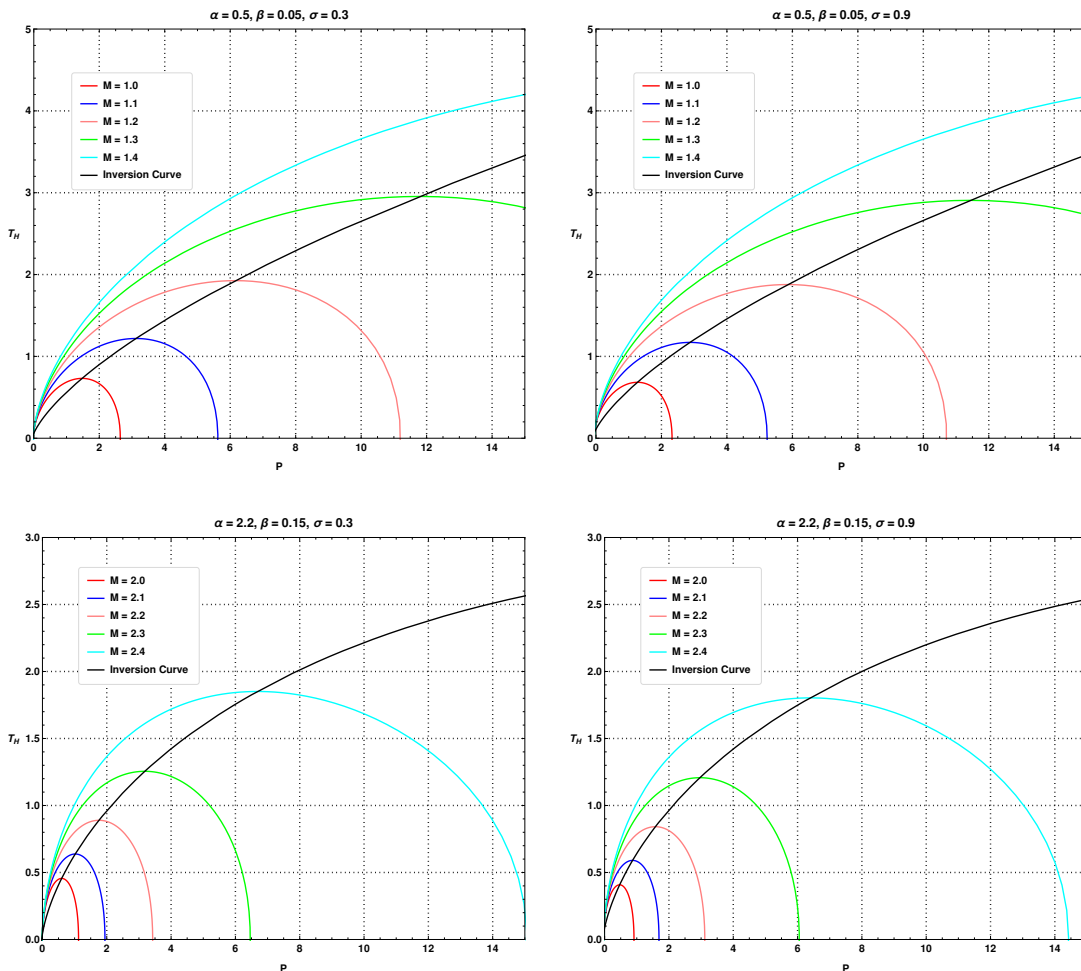


FIG. 4: Isenthalpic and inversion curves of the black hole.

Figures 4 and 5 illustrate the isenthalpic trajectories of the black hole in the (P, T) plane for various values of the model parameters, together with the corresponding inversion curves. For a fixed enthalpy M , each isenthalpic curve exhibits a characteristic behaviour: the temperature initially increases with pressure, reaches a maximum, and then decreases before intersecting the inversion curve. The point of intersection marks the transition between the heating ($\mu < 0$) and cooling ($\mu > 0$) phases during a Joule–Thomson expansion. Curves lying above the inversion line correspond to regimes in which the black hole cools under expansion, whereas those lying below indicate heating. The position and curvature of these isenthalpic trajectories therefore, encode detailed information about how the internal structure of the black hole responds to changes in the external thermodynamic variables.

The first two panels of Fig. 4 show the isenthalpic curves for $\alpha = 0.5$ and $\beta = 0.05$ for two different values of the quintessence parameter, $\sigma = 0.3$ and $\sigma = 0.9$. Increasing σ shifts the isenthalpic curves upward and slightly modifies the location of the turning points, although the overall shape remains similar. This behaviour is consistent with the earlier temperature analysis in Fig. 1, where larger σ was found to elevate the Hawking temperature, particularly in the small- and intermediate-radius regimes. The mild upward shift of the isenthalpic curves reflects the modest influence of the surrounding quintessence fluid on the thermal response of the black hole, in agreement with the small but positive shift observed in the inversion temperature in Fig. 3. Thus, for fixed values of α and β , the quintessence parameter affects the cooling–heating transition but only weakly, indicating that its thermodynamic effect is secondary to that of the intrinsic geometric parameters.

A more pronounced behaviour appears in the third and fourth panels, corresponding to $\alpha = 2.2$ and $\beta = 0.15$. In this regime, the isenthalpic curves display a stronger sensitivity to σ : the trajectories shift upward more substantially, and the departure between curves corresponding to different σ becomes more visible across the full pressure range. This amplification of the σ -dependence is consistent with the trends observed in earlier sections. Larger values of α and β were shown to enhance the repulsive or regularising effects in the near-horizon region, thereby modifying both the temperature minima and the divergence structure of the J-T coefficient. As a result, the external quintessence field interacts more strongly with the underlying geometry, producing a more significant shift in the cooling and heating regions. The combined behaviour confirms that the thermodynamic influence of σ becomes increasingly important when the deformation and nonlinear parameters are enhanced, demonstrating a nontrivial interplay between the intrinsic structure of the black hole and the surrounding exotic matter distribution.

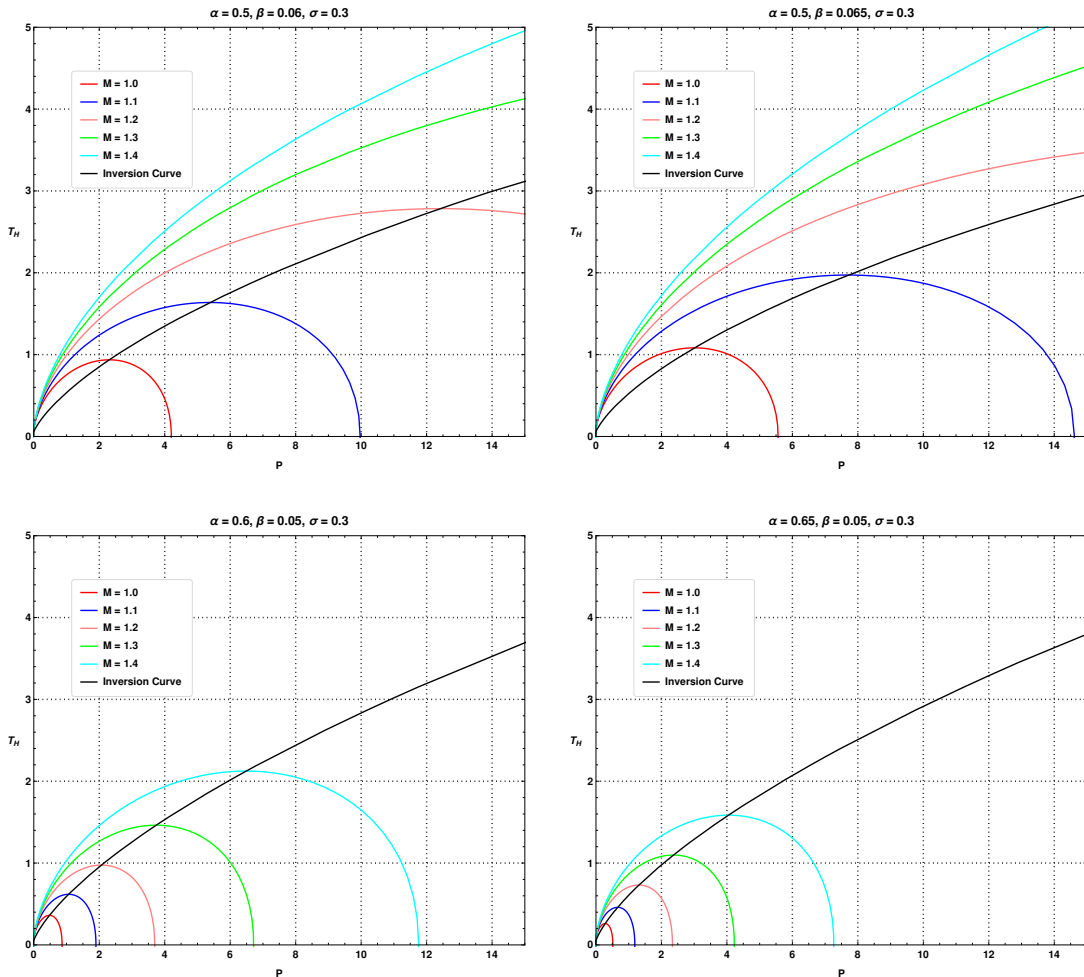


FIG. 5: Isenthalpic and inversion curves of the black hole.

Figure 5 further illustrates the behaviour of the isenthalpic curves in the (P, T) plane, focusing on the influence of the control parameter β and the deformation parameter α . The first two panels correspond to $\beta = 0.06$ and $\beta = 0.065$ with fixed $\alpha = 0.5$ and $\sigma = 0.3$. A clear trend emerges: increasing β causes the isenthalpic trajectories to expand outward, thereby increasing the area enclosed beneath each curve. Physically, this expansion reflects the enhanced nonlinear contributions associated with larger β , which modify the effective equation of state of the black hole. This behaviour is consistent with earlier findings from

the temperature plots and the inversion curves, where larger β elevated the temperature and shifted the inversion point. The increased area under the isenthalpic curves therefore confirms that the thermodynamic response of the black hole becomes more sensitive to pressure changes when nonlinear effects are strengthened.

The third and fourth panels show the isenthalpic curves for $\alpha = 0.6$ and $\alpha = 0.65$, keeping $\beta = 0.05$ and $\sigma = 0.3$ fixed. In contrast to the effect of β , increasing the deformation parameter α leads to a reduction in the area under the corresponding isenthalpic curves. This contraction indicates that higher values of α suppress the thermal response of the black hole at fixed enthalpy, a behaviour aligned with the shift of the temperature minimum and the earlier observation that α enhances the cooling region in the Joule–Thomson process. Since larger α introduces stronger geometric or regularisation effects near the horizon, the corresponding isenthalpic trajectories become more constrained, reducing the extent of the thermodynamic excursion in the (P, T) plane.

Together, the results in Fig. 5 reinforce the complementary roles played by α and β in the black-hole thermodynamics. While β amplifies the nonlinear matter-sector contributions and broadens the isenthalpic curves, α strengthens the geometric deformation and correspondingly contracts the accessible region of the (P, T) phase space. These trends are fully consistent with the behaviour observed in Figs. 1, 2, and 3, demonstrating a coherent interplay between the model parameters and the cooling–heating structure of the black hole.

IV. EFFICIENCY OF THE BLACK HOLE AS A THERMAL SYSTEM

A heat engine is any device or mechanism that converts heat into useful mechanical work. It gets energy from a source, which sits at a higher temperature, and after some part of this heat absorbed is converted to useful work, the rest amount of heat is transferred to the sink, which sits at a lower temperature. There is a working substance, usually a gas, expanding and contracting between some cycles of change, which facilitates the functioning of the system. More explicitly, it involves a closed-path process in the P-V plane involving absorption of heat Q_H from the source and eventually eliminating Q_C amount of heat to the sink. The work done is $W = Q_H - Q_C$. From the definition of efficiency of a heat engine, we have [90]

$$\eta = \frac{W}{Q_H}. \quad (23)$$

The maximum efficiency possible for a heat engine is theoretically the Carnot efficiency, given by [90]:

$$\eta_c = 1 - \frac{Q_C}{Q_H} = 1 - \frac{T_C}{T_H}. \quad (24)$$

Here, T_C and T_H represent the sink and source temperatures, respectively. In the case of static black hole system [90], it involves a simple reversible cycle with isotherms at higher and lower temperatures. Isothermal expansion involves the absorption of Q_H heat, and during the isothermal compression, Q_C heat is released. These paths are connected by adiabatic paths as can be seen from figure 6. For the sake of avoiding complications, we adopt a rectangular P-V cycle ($1 \rightarrow 2 \rightarrow 3 \rightarrow 4 \rightarrow 1$) as shown in figure 6. The amount of work done in one complete operating cycle of the black hole heat engine is mathematically stated as:

$$W_{net} = W_{1 \rightarrow 2} + W_{2 \rightarrow 3} + W_{3 \rightarrow 4} + W_{4 \rightarrow 1} = \frac{4}{3\sqrt{\pi}}(P_1 - P_4)\left(S_2^{\frac{3}{2}} - S_1^{\frac{3}{2}}\right). \quad (25)$$

Here, the terms P_1 and P_4 stand for pressure at states 1 and 4 of P-V cycle, respectively. Similarly, S_2 and S_1 represent the entropy of the system at states 2 and 1. As no heat exchange takes place in the isochoric processes, we compute heat absorbed during the isothermal expansion of the system Q_H , (during $1 \rightarrow 2$) as:

$$Q_H = \int_{T_1}^{T_2} C_P(P_1, T) dT = \int_{S_1}^{S_2} C_P\left(\frac{\partial T}{\partial S}\right) dS = \int_{S_1}^{S_2} T dS = M_2 - M_1. \quad (26)$$

$$Q_H = \frac{1}{6} \left[\frac{3(\sqrt{S_2} - \sqrt{S_1}) + 8P_1(S_2^{3/2} - S_1^{3/2})}{\sqrt{\pi}} + \alpha \left(\frac{\frac{3S_2}{\pi} + \frac{3\sqrt{S_2}\beta}{\sqrt{\pi}} + \beta^2}{\left(\frac{\sqrt{S_2}}{\sqrt{\pi}} + \beta\right)^3} - \frac{\frac{3S_1}{\pi} + \frac{3\sqrt{S_1}\beta}{\sqrt{\pi}} + \beta^2}{\left(\frac{\sqrt{S_1}}{\sqrt{\pi}} + \beta\right)^3} \right) + \frac{3\sigma(S_2 - S_1)}{\pi} \right] \quad (27)$$

The efficiency of the black hole heat engine is expressed as:

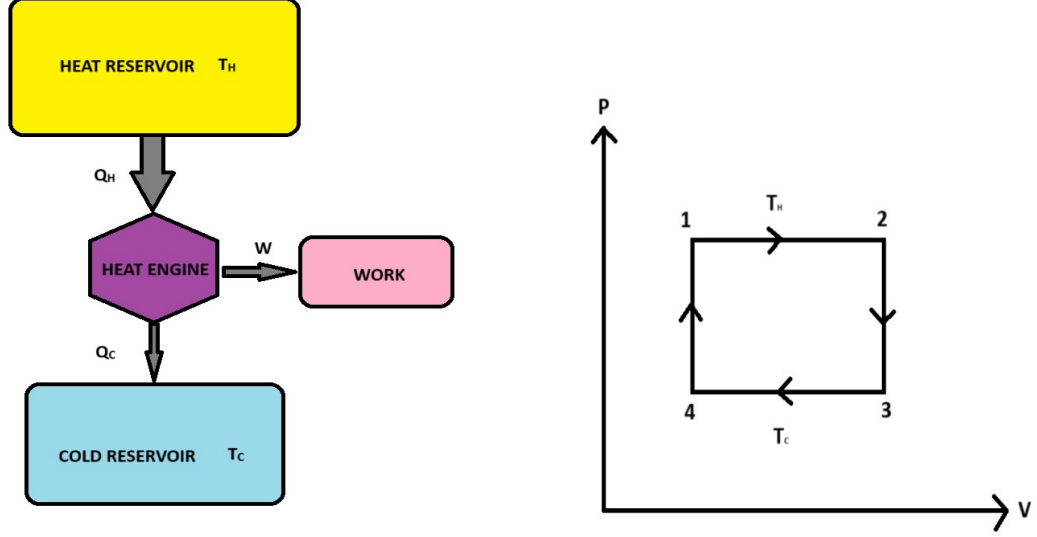


FIG. 6: A schematic figure of the working of a heat engine is shown. On the right, we have the Carnot engine P-V cycle.

$$\eta = \frac{8(P_1 - P_4)(S_2^{3/2} - S_1^{3/2})}{\sqrt{\pi} \left(-\frac{8P_1 S_1^{3/2}}{\sqrt{\pi}} + \frac{8P_1 S_2^{3/2}}{\sqrt{\pi}} - \frac{\alpha \left(\beta^2 + \frac{3\beta\sqrt{S_1} + 3S_1}{\sqrt{\pi}} \right)}{\left(\beta + \frac{\sqrt{S_1}}{\sqrt{\pi}} \right)^3} + \frac{\alpha \left(\beta^2 + \frac{3\beta\sqrt{S_2} + 3S_2}{\sqrt{\pi}} \right)}{\left(\beta + \frac{\sqrt{S_2}}{\sqrt{\pi}} \right)^3} - \frac{3\sigma S_1}{\pi} + \frac{3\sigma S_2}{\pi} + \frac{3\sqrt{S_2}}{\sqrt{\pi}} - \frac{3\sqrt{S_1}}{\sqrt{\pi}} \right)} \quad (28)$$

The following figure 7 shows the variation of efficiency versus entropy S_2 for different values of deformation parameter α . It is seen that with increasing α , efficiency shows a fair bit of variation for smaller S_2 . After that, the curves converge, and efficiency becomes constant at about 90%. Lower α implies lower efficiency. The next plot shows the variation of efficiency with β . We observed that efficiency is larger for smaller values of the control parameter β , before converging to 88% for all the graphs. The third plot shows the variation of efficiency with quintessence parameter σ . It is seen that efficiency rises to about 80% for very smaller values of S_2 , then decreases for all cases. It also converges to about 52% efficiency with increasing S_2 . Lower σ leads to higher efficiency. It is worth mentioning that though we do not encounter negative efficiency, this may imply a reverse heat engine cycle, behaving like a refrigerator.

In the next Figure 8, variation of efficiency with deformation parameter α is analysed with various values of the control parameter β and pressure P_1 respectively. As can be seen from the left plot, the efficiency increases more rapidly for smaller β values. Efficiency increases with increasing P_1 as seen from the graph. Similarly, the Figure 9 shows variation of efficiency versus β for various values of pressure P_1 and quintessence parameter σ respectively. Efficiency decreases with β and it is also seen from the first plot that efficiency is higher for larger pressure. Similarly, efficiency is larger for smaller quintessence parameter σ as can be clearly inferred from the plot.

The expression for Carnot efficiency is found out to be:

$$\eta_c = 1 - \frac{T_C}{T_H} = 1 - \frac{\frac{\pi(8P_1 S_1 + 1)}{\sqrt{S_1}} + 2\sqrt{\pi}\sigma - \frac{\alpha\sqrt{S_1}}{\left(\beta + \frac{\sqrt{S_1}}{\sqrt{\pi}}\right)^4}}{\frac{\pi(8P_1 S_2 + 1)}{\sqrt{S_2}} + 2\sqrt{\pi}\sigma - \frac{\alpha\sqrt{S_2}}{\left(\beta + \frac{\sqrt{S_2}}{\sqrt{\pi}}\right)^4}} \quad (29)$$

The ratio of efficiency to Carnot efficiency is plotted for different values of quintessence parameter σ , deformation parameters α and control parameter β respectively, as shown in the figure 10. The steps of computation can be followed from Ref. [90]. The first plot displays efficiency ratio $\frac{\eta}{\eta_c}$ versus S_2 for different values of quintessence parameter σ . The efficiency ratio increases as σ increases. The second plot displays the efficiency ratio versus entropy S_2 for various values of α . The efficiency ratio increases as α decreases. Third plot is efficiency ratio versus S_2 for different control parameter values. Except for $\beta = 0.1$, higher β values signify higher efficiency ratio. The values of the parameters chosen have also been mentioned in the plots. It is also important to note that the chosen values of the parameters are for the proper display of the results and further study has to

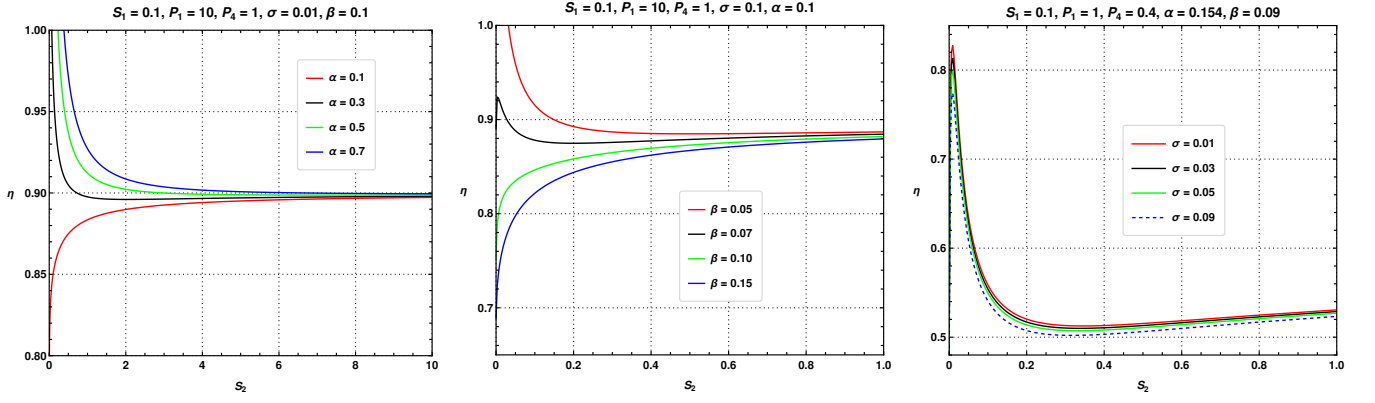


FIG. 7: The efficiency of a deformed AdS-Schwarzschild black hole in the presence of quintessence field is shown in the plots. We analyse the variation of efficiency with respect to S_2 for different values of deformation parameters α and β , and quintessence parameter σ in the plots.

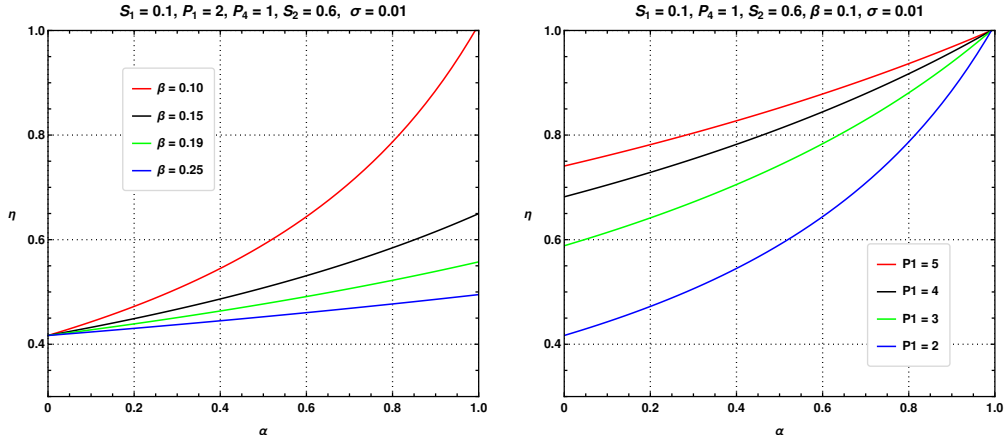


FIG. 8: The efficiency of a deformed AdS-Schwarzschild black hole in the presence of quintessence field is shown in the plot. The variation of efficiency with α is analysed with different values of β and pressure term P_1 is shown.

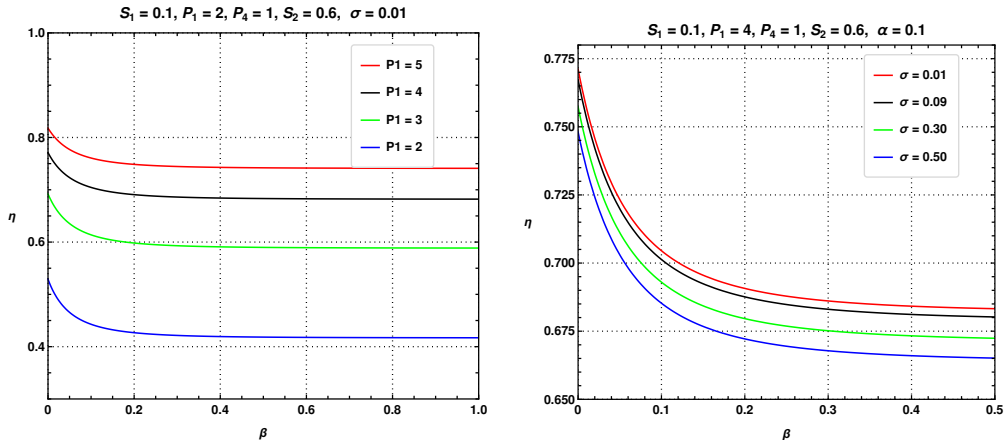


FIG. 9: The efficiency of a deformed AdS-Schwarzschild black hole in the presence of quintessence field is shown in the plots. The variation of efficiency with β is analysed with different values of P_1 and pressure term σ is shown.

be done to constrain the exact range of the parameters. In this analysis, we can see some tentative ranges of parameters beyond which efficiency is going towards negative range. This may indicate that the black hole heat engine might not be feasible in that

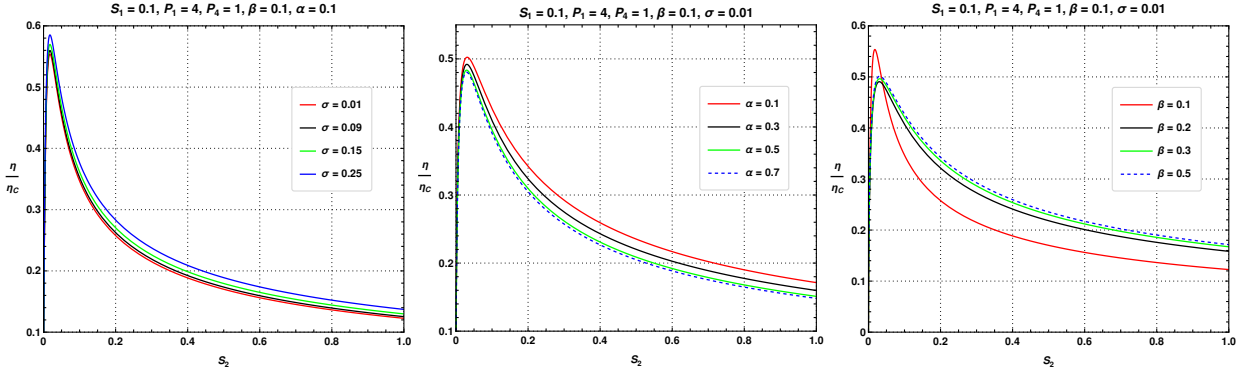


FIG. 10: Ratio of efficiency to Carnot efficiency of a deformed AdS-Schwarzschild black hole in the presence of quintessence field is shown in the plots. Variation with S_2 is displayed for different values of σ , α and β respectively.

regime of parameter values.

TABLE I: Numerical values of efficiency and the ratio of efficiency to Carnot efficiency for the black hole heat engine. Parameters used: $P_4 = 1$, $S_2 = 0.6$, $S_1 = 0.1$

P_1	α	β	σ	η/η_c	η
2.0	0.1	0.1	0.01	0.3006	0.4428
3.0	0.1	0.1	0.01	0.2056	0.6138
2.0	0.3	0.1	0.01	0.0529	0.5061
2.0	0.3	0.3	0.01	0.3813	0.4312
2.0	0.1	0.1	0.05	0.3030	0.4409

The tabular presentation of η/η_c and η for some particular values of deformation parameters α , control parameter β and quintessence parameter σ has been shown in Table I. The values of efficiency (ratio) and its dependence on the model parameters is shown, which is clearly visible from Figure 10. Parameter values are chosen such that the efficiency remains rational and positive.

V. CONCLUDING REMARKS

In this work, we have investigated the J-T expansion and the extended thermodynamic behaviour of a black hole modified by the deformation parameter α , control parameter β , and quintessence parameter σ . By analysing the Hawking temperature, the J-T coefficient, the inversion curves, and the associated isenthalpic trajectories, we obtained a comprehensive picture of how these parameters influence both the microscopic structure and macroscopic thermal response of the system.

The temperature analysis revealed that all three parameters significantly affect the location and depth of the temperature minimum, thereby modifying the thermal stability of small black holes. An increase in α or β shifts the temperature minimum to larger horizon radii, whereas σ predominantly elevates the temperature in the small-radius regime. Correspondingly, the behaviour of the J-T coefficient exhibits divergences whose locations and signs are in agreement with these temperature trends: larger values of α and β enlarge the cooling region, while σ produces a milder but consistent shift in the heating-cooling transition. These observations confirm that the cooling and heating characteristics of the black hole are tightly linked to the interplay between geometric deformation, nonlinear matter coupling, and external exotic fluid.

The inversion curves further solidify this thermodynamic picture. Both α and β raise the inversion temperature across the full pressure range, indicating that the black hole requires higher temperatures to undergo the transition between heating and cooling when the deformation or nonlinear effects are stronger. Although the influence of σ on the inversion temperature is comparatively weak, it remains positive and consistent with its effect on the Hawking temperature and the J-T coefficient. The isenthalpic analysis also reveals clear trends: increasing β expands the isenthalpic trajectories, while increasing α compresses them, demonstrating opposite but complementary roles played by the two intrinsic parameters in shaping the thermodynamic phase space.

The black hole heat engine is theorised, and the efficiency is analysed for variation of model parameters. The deformation parameter α increases the efficiency, while a higher β value leads to lower efficiency of the heat engine. Heat engine efficiency

has an inverse relation with quintessence parameter σ .

By comparing our results with past related works, several fundamental physical consequences emerge that distinguish this deformed configuration from both standard General Relativity and other regular black hole models. Most notably, our heat engine analysis reveals a contrasting behavior: while past studies, such as those on the Bardeen-AdS black hole [90], demonstrate that a quintessence field enhances thermodynamic efficiency, our deformed model shows the exact opposite. Specifically, both the quintessence parameter σ and the control parameter β actively reduce the heat engine's efficiency. Furthermore, our model exhibits a unique competing thermodynamic interplay in the (P, T) phase space that cannot be captured by standard GR. The deformation parameter α contracts the accessible area under the isenthalpic curves, thereby suppressing the thermal response, whereas β amplifies nonlinear matter-sector contributions, causing these trajectories to expand outward. Ultimately, these geometric and matter-field corrections act collectively to govern the inversion mechanism, forcing the black hole to require higher temperatures to trigger the heating-cooling transition. This unified thermodynamic structure underscores the profound differences between our specific deformed configuration and previously studied regular black holes.

Taken together, these results demonstrate that the thermodynamic and J-T properties of the black hole are highly sensitive to modifications introduced by α , β , and σ . The coherent agreement between the temperature profiles, J-T coefficient behaviour, inversion curves, and isenthalpic trajectories provides strong evidence that the extended phase structure is governed by a unified underlying mechanism shaped by geometric and matter-field corrections. This study not only deepens our understanding of modified black-hole thermodynamics but also opens avenues for exploring analogous phenomena in other regular, nonlinear, or exotic-matter-supported gravitational systems. Future work may involve analysing critical behaviour, microstructure interactions, or quantum corrections within this framework, potentially revealing further connections between modified gravity and black-hole heat-engine physics.

ACKNOWLEDGMENTS

DJG acknowledges the contribution of the COST Action CA21136 – “Addressing observational tensions in cosmology with systematics and fundamental physics (CosmoVerse)”. RK is thankful to Prof. U. D. Goswami for his mentorship during RK's early days of research.

DATA AVAILABILITY STATEMENT

There are no new data associated with this article.

-
- [1] E. Witten, Introduction to black hole thermodynamics, *Eur. Phys. J. Plus* **140**, 430 (2025), [arXiv:2412.16795 \[hep-th\]](#).
 - [2] A. Einstein, The Field Equations of Gravitation, *Sitzungsber. Preuss. Akad. Wiss. Berlin (Math. Phys.)* **1915**, 844 (1915).
 - [3] T. P. Sotiriou and V. Faraoni, $f(R)$ Theories Of Gravity, *Rev. Mod. Phys.* **82**, 451 (2010), [arXiv:0805.1726 \[gr-qc\]](#).
 - [4] D. Hansen, D. Kubiznak, and R. B. Mann, Universality of P-V Criticality in Horizon Thermodynamics, *JHEP* **01**, 047, [arXiv:1603.05689 \[gr-qc\]](#).
 - [5] R.-G. Cai, Y.-P. Hu, Q.-Y. Pan, and Y.-L. Zhang, Thermodynamics of Black Holes in Massive Gravity, *Phys. Rev. D* **91**, 024032 (2015), [arXiv:1409.2369 \[hep-th\]](#).
 - [6] S. Carlip, Black Hole Thermodynamics, *Int. J. Mod. Phys. D* **23**, 1430023 (2014), [arXiv:1410.1486 \[gr-qc\]](#).
 - [7] S. Soroushfar, A. I. Kashkooli, H. Farahani, P. Rudra, and B. Pourhassan, Geodesics and thermodynamics of Einstein-Power-Yang–Mills AdS black holes, *Phys. Dark Univ.* **47**, 101800 (2025).
 - [8] R. Karmakar and U. D. Goswami, Quasinormal modes, thermodynamics and shadow of black holes in Hu–Sawicki $f(R)$ gravity theory, *Eur. Phys. J. C* **84**, 969 (2024), [arXiv:2406.18329 \[gr-qc\]](#).
 - [9] D. J. Gogoi, P. Hazarika, J. Bora, and R. Changmai, Thermodynamics of Deformed AdS-Schwarzschild Black Holes in the Presence of Thermal Fluctuations, *Fortsch. Phys.* **73**, e70004 (2025), [arXiv:2501.15629 \[hep-th\]](#).
 - [10] N. J. Gogoi, D. J. Gogoi, and J. Bora, Topology of 5-dimensional Einstein–Gauss–Bonnet AdS black hole thermodynamics surrounded by a cloud of Strings, *Phys. Dark Univ.* **50**, 102099 (2025).
 - [11] J. D. Bekenstein, Black holes and the second law, *Lett. Nuovo Cim.* **4**, 737 (1972).
 - [12] S. Bora, D. J. Gogoi, and P. K. Karmakar, Impact of Thermodynamic Corrections on the Stability of Hayward-Anti de Sitter Black Hole Surrounded by a Fluid of Strings, (2025), [arXiv:2510.04208 \[gr-qc\]](#).
 - [13] C. Fang, J. Jiang, and M. Zhang, Revisiting thermodynamic topologies of black holes, *JHEP* **01**, 102, [arXiv:2211.15534 \[gr-qc\]](#).
 - [14] S.-W. Wei, Y.-X. Liu, and R. B. Mann, Black Hole Solutions as Topological Thermodynamic Defects, *Phys. Rev. Lett.* **129**, 191101 (2022), [arXiv:2208.01932 \[gr-qc\]](#).
 - [15] P. K. Yerra and C. Bhamidipati, Topology of Born-Infeld AdS black holes in 4D novel Einstein-Gauss-Bonnet gravity, *Phys. Lett. B* **835**, 137591 (2022), [arXiv:2207.10612 \[gr-qc\]](#).

- [16] S.-W. Wei and Y.-X. Liu, Topology of black hole thermodynamics, *Phys. Rev. D* **105**, 104003 (2022), [arXiv:2112.01706 \[gr-qc\]](#).
- [17] Ö. Ökcü and E. Aydiner, Joule–Thomson expansion of the charged AdS black holes, *Eur. Phys. J. C* **77**, 24 (2017), [arXiv:1611.06327 \[gr-qc\]](#).
- [18] D. J. Gogoi, Y. Sekhmani, S. Bora, J. Rayimbaev, J. Bora, and R. Myrzakulov, Corrected thermodynamics and stability of magnetic charged AdS black holes surrounded by quintessence, *JCAP* **11**, 019, [arXiv:2407.10946 \[gr-qc\]](#).
- [19] Y. Sekhmani, D. J. Gogoi, R. Myrzakulov, and J. Rayimbaev, Phase structures and critical behavior of rational non-linear electrostatics Anti de Sitter black holes in Rastall gravity, *Commun. Theor. Phys.* **76**, 045403 (2024), [arXiv:2403.04888 \[gr-qc\]](#).
- [20] S. I. Kruglov, Magnetically Charged AdS Black Holes and Joule–Thomson Expansion, *Grav. Cosmol.* **29**, 57 (2023), [arXiv:2304.02121 \[physics.gen-ph\]](#).
- [21] M. Tataryn and M. Stetsko, Thermodynamics of a static electric-magnetic black hole in Einstein-Born-Infeld-AdS theory with different horizon geometries, *Gen. Rel. Grav.* **53**, 72 (2021), [arXiv:2304.02753 \[gr-qc\]](#).
- [22] A. Dehghani, B. Pourhassan, S. Zarepour, and E. N. Saridakis, Thermodynamic schemes of charged BTZ-like black holes in arbitrary dimensions, *Phys. Dark Univ.* **42**, 101371 (2023), [arXiv:2305.08219 \[hep-th\]](#).
- [23] S. I. Kruglov, Magnetic black holes within Einstein–AdS gravity coupled to nonlinear electrostatics, extended phase space thermodynamics and Joule–Thomson expansion, *Can. J. Phys.* **101**, 739 (2023), [arXiv:2401.15115 \[physics.gen-ph\]](#).
- [24] M. R. Alipour, S. Noori Gashti, M. A. S. Afshar, and J. Sadeghi, Cooling and heating regions of Joule-Thomson expansion for AdS black holes: Einstein-Maxwell-power-Yang-Mills and Kerr Sen black holes, *Gen. Rel. Grav.* **57**, 61 (2025), [arXiv:2402.02257 \[hep-th\]](#).
- [25] R.-B. Wang, S.-J. Ma, L. You, Y.-C. Tang, Y.-H. Feng, X.-R. Hu, and J.-B. Deng, Thermodynamics of AdS-Schwarzschild-like black hole in loop quantum gravity, *Eur. Phys. J. C* **84**, 1161 (2024), [arXiv:2405.08241 \[gr-qc\]](#).
- [26] S. I. Kruglov, Einstein-AdS Gravity Coupled to Nonlinear Electrostatics, Magnetic Black Holes, Thermodynamics in an Extended Phase Space and Joule–Thomson Expansion, *Universe* **9**, 456 (2023), [arXiv:2408.04714 \[physics.gen-ph\]](#).
- [27] R.-B. Wang, S.-J. Ma, L. You, J.-B. Deng, and X.-R. Hu, Thermodynamics of Schwarzschild-AdS black hole in non-commutative geometry, *Chin. Phys. C* **49**, 065101 (2025), [arXiv:2410.03650 \[gr-qc\]](#).
- [28] H. R. Bakhtiarzadeh, Joule-Thomson expansion and heat engine efficiency of charged rotating black strings, *Gen. Rel. Grav.* **57**, 146 (2025), [arXiv:2508.09712 \[gr-qc\]](#).
- [29] G. Fatima, A. Eid, J. Rayimbaev, and S. Muminov, Joule–Thomson expansion of black hole in Cotton gravity coupled to nonlinear electrostatics, *Phys. Dark Univ.* **49**, 102045 (2025).
- [30] E. Dai, F. Javed, A. Waseem, M. Alosaimi, and R. M. Zulqarnain, Thermodynamic insights into Joule–Thomson expansion, particle dynamics, and emission energy of AdS black holes in Horndeski theory, *Phys. Dark Univ.* **49**, 102014 (2025).
- [31] R.-B. Wang, L. You, S.-J. Ma, J.-B. Deng, and X.-R. Hu, Thermodynamic phase transition and Joule-Thomson expansion of a quantum corrected black hole in AdS spacetime, *Chin. Phys.* **49**, 115102 (2025), [arXiv:2504.06907 \[gr-qc\]](#).
- [32] N. Media and T. I. Singh, Joule-Thomson Expansion of Kerr-Newman-de Sitter Black Hole Under Lorentz Violation Theory, *Int. J. Theor. Phys.* **64**, 82 (2025).
- [33] Ö. Ökcü and E. Aydiner, Joule–Thomson expansion of Kerr–AdS black holes, *Eur. Phys. J. C* **78**, 123 (2018), [arXiv:1709.06426 \[gr-qc\]](#).
- [34] H. Ghaffarnejad, E. Yaraie, and M. Farsam, Quintessence Reissner Nordström Anti de Sitter Black Holes and Joule Thomson effect, *Int. J. Theor. Phys.* **57**, 1671 (2018), [arXiv:1802.08749 \[gr-qc\]](#).
- [35] M. Chabab, H. El Moumni, S. Iraoui, K. Masmar, and S. Zhizeh, Joule-Thomson Expansion of RN-AdS Black Holes in $f(R)$ gravity, *LHEP* **02**, 05 (2018), [arXiv:1804.10042 \[gr-qc\]](#).
- [36] M. Rostami, J. Sadeghi, S. Miraboutalebi, A. A. Masoudi, and B. Pourhassan, Charged accelerating AdS black hole of $f(R)$ gravity and the Joule–Thomson expansion, *Int. J. Geom. Meth. Mod. Phys.* **17**, 2050136 (2020), [arXiv:1908.08410 \[gr-qc\]](#).
- [37] B. Hamil, B. C. Lütfüoğlu, and L. Dahbi, Quantum-corrected Schwarzschild AdS black hole surrounded by quintessence: Thermodynamics and shadows, *Mod. Phys. Lett. A* **39**, 2450161 (2024), [arXiv:2307.16287 \[gr-qc\]](#).
- [38] M. Yasir, X. Tiecheng, F. Javed, and G. Mustafa, Thermal analysis and Joule-Thomson expansion of black hole exhibiting metric-affine gravity*, *Chin. Phys. C* **48**, 015103 (2024), [arXiv:2305.13709 \[gr-qc\]](#).
- [39] M.-Y. Zhang, H. Chen, H. Hassanabadi, Z.-W. Long, and H. Yang, Joule-Thomson expansion of charged dilatonic black holes*, *Chin. Phys. C* **47**, 045101 (2023), [arXiv:2209.00868 \[gr-qc\]](#).
- [40] M.-Y. Zhang, H. Chen, H. Hassanabadi, Z.-W. Long, and H. Yang, Critical behavior and Joule-Thomson expansion of charged AdS black holes surrounded by exotic fluid with modified Chaplygin equation of state*, *Chin. Phys. C* **48**, 065101 (2024), [arXiv:2401.17589 \[gr-qc\]](#).
- [41] R. H. Ali, G. Abbas, A. Jawad, B. S. Alkahtani, and G. Mustafa, Mathematical formalism of Joule-Thomson process for ADS-RN black hole coupled with non-linear electrostatics field, *Nucl. Phys. B* **1010**, 116735 (2025).
- [42] S. Chaudhary, A. Jawad, and M. Yasir, Thermodynamic geometry and Joule-Thomson expansion of black holes in modified theories of gravity, *Phys. Rev. D* **105**, 024032 (2022).
- [43] A. Jawad, M. Yasir, and S. Rani, Joule–Thomson expansion and quasinormal modes of regular non-minimal magnetic black hole, *Mod. Phys. Lett. A* **35**, 2050298 (2020).
- [44] S. Rani, H. Riaz, U. Zafar, A. Jawad, N. Myrzakulov, and S. Shaymatov, Stability and topological thermodynamics of black holes through modified entropy, *Eur. Phys. J. C* **85**, 971 (2025).
- [45] S. Rani, A. Jawad, M. Heydari-Fard, and U. Zafar, Thermodynamic and shadow analysis of Dehnen type dark matter Halo corrected Schwarzschild black hole surrounded by thin disk, *Eur. Phys. J. C* **85**, 677 (2025).
- [46] S. Rani, A. Jawad, H. Raza, S. Shaymatov, M. Muzaffar, and H. Riaz, Thermodynamic properties and geometries of bardeen black hole surrounded by string clouds, *Eur. Phys. J. C* **84**, 904 (2024).
- [47] D. J. Gogoi, Y. Sekhmani, D. Kalita, N. J. Gogoi, and J. Bora, Joule-Thomson Expansion and Optical Behaviour of Reissner-Nordström-Anti-de Sitter Black Holes in Rastall Gravity Surrounded by a Quintessence Field, *Fortsch. Phys.* **71**, 2300010 (2023), [arXiv:2306.02881 \[gr-qc\]](#).

- [48] P. Paul, S. Upadhyay, and D. V. Singh, Charged AdS black holes in 4D Einstein–Gauss–Bonnet massive gravity, *Eur. Phys. J. Plus* **138**, 566 (2023), [arXiv:2307.09198 \[gr-qc\]](#).
- [49] Y. Ladghami, A. Bargach, A. Bouali, T. Ouali, and G. Mustafa, Spacetime foam effects on charged AdS black hole thermodynamics, *Nucl. Phys. B* **1018**, 117015 (2025), [arXiv:2411.06271 \[hep-th\]](#).
- [50] F. Ahmed, S. Noori Gashti, B. Pourhassan, and A. Bouzenada, Thermodynamics and Joule–Thomson expansion of Schwarzschild-AdS black holes with a cloud of strings and quintessential-like fluid, *Eur. Phys. J. C* **85**, 1149 (2025), [arXiv:2508.12318 \[gr-qc\]](#).
- [51] F. Javed, M. Zeeshan Gul, O. Donmez, T. Naseer, and M. H. Alshehri, Joule-Thomson expansion with Barrow entropy and particle dynamics of charged Rastall-AdS black hole, *Nucl. Phys. B* **1018**, 117001 (2025).
- [52] A. Waseem, F. Javed, G. Mustafa, S. K. Maurya, F. Atamurotov, and M. Shrahili, Joule–Thomson expansion of Hayward-AdS black hole surrounded by fluid of strings, *Annals Phys.* **480**, 170087 (2025).
- [53] F. Liu, Y.-Z. Du, R. Zhao, and H.-F. Li, The phase transitions and Joule–Thomson processes of charged de Sitter black holes with cloud of string and quintessence, *Chin. J. Phys.* **95**, 371 (2025).
- [54] F. Javed, A. Waseem, P. Channuie, G. Mustafa, T. Muhammad, and E. Güdekli, Particle dynamics and Joule–Thomson expansion of phantom anti-de Sitter black hole stability and thermal fluctuations in massive gravity, *Phys. Dark Univ.* **47**, 101766 (2025).
- [55] T.-Y. Liu, Joule-thomson expansion of vanished cooling region for five-dimensional neutral Gauss-Bonnet AdS black hole, *Gen. Rel. Grav.* **56**, 140 (2024).
- [56] G. Mustafa, F. Javed, S. K. Maurya, S. Alkarni, O. Donmez, A. Cilli, and E. Güdekli, Joule-Thomson expansion, motion of particles and QPOs around Bardeen-AdS black hole immersed in a fluid of strings, *JHEAp* **44**, 437 (2024).
- [57] F. Javed, G. Mustafa, G. Fatima, S. K. Maurya, M. H. Alshehri, and I. Mubeen, Joule-Thomson expansion for charged-AdS black hole with nonlinear electrodynamics and thermal fluctuations by using Barrow entropy, *JHEAp* **44**, 60 (2024).
- [58] A. H. Rezaei and K. Nozari, Joule–Thomson expansion in a mimetic black hole, *Sci. Rep.* **14**, 19475 (2024).
- [59] M. Yasir, T. Xia, A. Ditta, D. Arora, F. Atamurotov, A. Mahmood, and O. Egamberdiev, Joule–Thomson expansion of Bardeen black hole with a cloud of strings, *Int. J. Mod. Phys. A* **39**, 2450046 (2024).
- [60] K. Masmar, Joule–Thomson expansion for a nonlinearly charged Anti-de Sitter black hole, *Int. J. Geom. Meth. Mod. Phys.* **20**, 2350080 (2023).
- [61] Y. Sekhmani, Z. Dahbi, A. Najim, and A. Waqdim, Joule–Thomson expansion of 5-dimensional R-charged black holes, *Annals Phys.* **444**, 169060 (2022).
- [62] Q.-M. Feng, J. Pu, and Q.-Q. Jiang, Effects of magnetic monopole charge on Joule–Thomson expansion of regular Ayón Beato–García black hole, *Class. Quant. Grav.* **39**, 155007 (2022).
- [63] J. Barrientos and J. Mena, Joule-Thomson expansion of AdS black holes in quasitopological electromagnetism, *Phys. Rev. D* **106**, 044064 (2022), [arXiv:2206.06018 \[gr-qc\]](#).
- [64] S. I. Kruglov, Nonlinearly charged AdS black holes, extended phase space thermodynamics and Joule–Thomson expansion, *Annals Phys.* **441**, 168894 (2022), [arXiv:2208.13662 \[physics.gen-ph\]](#).
- [65] J.-T. Xing, Y. Meng, and X.-M. Kuang, Joule-Thomson expansion for hairy black holes, *Phys. Lett. B* **820**, 136604 (2021).
- [66] Y. Meng, B. B. Chen, and J. Tang, Cooling–heating phase transition of the Euler–Heisenberg-AdS black hole, *Mod. Phys. Lett. A* **36**, 2150165 (2021).
- [67] J. P. M. Graça, E. F. Capossoli, and H. Boschi-Filho, Joule-Thomson expansion for noncommutative uncharged black holes, *EPL* **135**, 41002 (2021), [arXiv:2107.05781 \[hep-th\]](#).
- [68] A. Biswas, Joule-Thomson expansion of AdS black holes in Einstein Power-Yang-mills gravity, *Phys. Scripta* **96**, 125310 (2021), [arXiv:2106.11066 \[gr-qc\]](#).
- [69] C.-M. Zhang, M. Zhang, and D.-C. Zou, Joule–Thomson expansion of Born–Infeld AdS black holes in consistent 4D Einstein–Gauss–Bonnet gravity, *Mod. Phys. Lett. A* **37**, 2250063 (2022), [arXiv:2106.00183 \[hep-th\]](#).
- [70] R. Yin, J. Liang, and B. Mu, Joule–Thomson expansion of Reissner–Nordström-Anti-de Sitter black holes with cloud of strings and quintessence, *Phys. Dark Univ.* **34**, 100884 (2021), [arXiv:2105.09173 \[gr-qc\]](#).
- [71] J. P. Morais Graça, E. Folco Capossoli, H. Boschi-Filho, and I. P. Lobo, Joule-Thomson expansion for quantum corrected AdS-Reissner–Nordström black holes in a Kiselev spacetime, *Phys. Rev. D* **107**, 024045 (2023), [arXiv:2105.04689 \[gr-qc\]](#).
- [72] J. Liang, B. Mu, and P. Wang, Joule-Thomson expansion of lower-dimensional black holes, *Phys. Rev. D* **104**, 124003 (2021), [arXiv:2104.08841 \[gr-qc\]](#).
- [73] K. V. Rajani, C. L. A. Rizwan, A. Naveena Kumara, M. S. Ali, and D. Vaid, Joule–Thomson expansion of regular Bardeen AdS black hole surrounded by static anisotropic matter field, *Phys. Dark Univ.* **32**, 100825 (2021), [arXiv:2002.03634 \[gr-qc\]](#).
- [74] S.-Q. Lan, Joule-Thomson expansion of neutral AdS black holes in massive gravity, *Nucl. Phys. B* **948**, 114787 (2019).
- [75] C. H. Nam, Heat engine efficiency and Joule–Thomson expansion of nonlinear charged AdS black hole in massive gravity, *Gen. Rel. Grav.* **53**, 30 (2021), [arXiv:1906.05557 \[gr-qc\]](#).
- [76] D. Mahdavian Yekta, A. Hadikhani, and Ö. Ökcü, Joule-Thomson expansion of charged AdS black holes in Rainbow gravity, *Phys. Lett. B* **795**, 521 (2019), [arXiv:1905.03057 \[hep-th\]](#).
- [77] A. Rizwan C. L., N. Kumara A., D. Vaid, and K. M. Ajith, Joule-Thomson expansion in AdS black hole with a global monopole, *Int. J. Mod. Phys. A* **33**, 1850210 (2019), [arXiv:1805.11053 \[gr-qc\]](#).
- [78] J.-X. Mo, G.-Q. Li, S.-Q. Lan, and X.-B. Xu, Joule-Thomson expansion of d -dimensional charged AdS black holes, *Phys. Rev. D* **98**, 124032 (2018), [arXiv:1804.02650 \[gr-qc\]](#).
- [79] P. Paul and S. I. Kruglov, Magnetic black holes in 4D Einstein–Gauss–Bonnet massive gravity coupled to nonlinear electrodynamics, *Int. J. Geom. Meth. Mod. Phys.* **22**, 2450330 (2025), [arXiv:2403.02056 \[gr-qc\]](#).
- [80] C. V. Johnson and F. Rosso, Holographic Heat Engines, Entanglement Entropy, and Renormalization Group Flow, *Class. Quant. Grav.* **36**, 015019 (2019), [arXiv:1806.05170 \[hep-th\]](#).
- [81] R. Penrose, Gravitational collapse: The role of general relativity, *Riv. Nuovo Cim.* **1**, 252 (1969).

- [82] M. R. Setare and H. Adami, Polytropic black hole, *Phys. Rev. D* **91**, 084014 (2015).
- [83] C. V. Johnson, Born–Infeld AdS black holes as heat engines, *Class. Quant. Grav.* **33**, 135001 (2016), [arXiv:1512.01746 \[hep-th\]](#).
- [84] S. H. Hendi, B. Eslam Panah, S. Panahiyan, H. Liu, and X. H. Meng, Black holes in massive gravity as heat engines, *Phys. Lett. B* **781**, 40 (2018), [arXiv:1707.02231 \[hep-th\]](#).
- [85] J.-X. Mo, F. Liang, and G.-Q. Li, Heat engine in the three-dimensional spacetime, *JHEP* **03**, 010, [arXiv:1701.00883 \[gr-qc\]](#).
- [86] T. Roy and U. Debnath, Van der Waals black hole as a heat engine, *Int. J. Mod. Phys. A* **36**, 2150114 (2021).
- [87] C. Nag, T. Roy, and U. Debnath, Thermodynamics of modified Bardeen–AdS black hole: Heat engine, *Int. J. Geom. Meth. Mod. Phys.* **20**, 2350093 (2023).
- [88] T. Roy, A. Sardar, and U. Debnath, Thermodynamic overview and heat engine efficiency of Kerr–Sen–AdS black hole, *Int. J. Geom. Meth. Mod. Phys.* **20**, 2350136 (2023).
- [89] G. Fatima, F. Javed, A. Waseem, B. Almutairi, G. Mustafa, F. Atamurotov, and E. Güdekli, Heat engine efficiency, particle dynamics and thermodynamic properties of Hayward–Letelier-AdS Black Hole, *Phys. Dark Univ.* **47**, 101820 (2025).
- [90] K. V. Rajani, C. L. Ahmed Rizwan, A. Naveena Kumara, D. Vaid, and K. M. Ajith, Regular Bardeen AdS black hole as a heat engine, *Nucl. Phys. B* **960**, 115166 (2020), [arXiv:1904.06914 \[gr-qc\]](#).
- [91] M. R. Khosravipoor and M. Farhoudi, Thermodynamics of deformed AdS-Schwarzschild black hole, *Eur. Phys. J. C* **83**, 1045 (2023), [arXiv:2311.02456 \[gr-qc\]](#).
- [92] D. Bini, A. Geralico, and R. P. Kerr, The Kerr-Schild ansatz revised, *Int. J. Geom. Meth. Mod. Phys.* **7**, 693 (2010), [arXiv:1408.4601 \[gr-qc\]](#).
- [93] M. Shahjalal, Thermodynamics of quantum-corrected Schwarzschild black hole surrounded by quintessence, *Nucl. Phys. B* **940**, 63 (2019).
- [94] F. Ahmed, A. Al-Badawi, İ. Sakallı, and D. J. Gogoi, Geodesics and scalar perturbations of deformed AdS-Schwarzschild black hole with a global monopole surrounded by a quintessence field, (2025), [arXiv:2505.12122 \[gr-qc\]](#).
- [95] J. M. Bardeen, B. Carter, and S. W. Hawking, The Four laws of black hole mechanics, *Commun. Math. Phys.* **31**, 161 (1973).